Supporting Information

Eagle et al. 10.1073/pnas.0911115107

SI Text

Modeling ^{13}C-^{18}O Clumping in Apatite—Methods and Results. An initial theoretical thermodynamic model of the ^{13}C-^{18}O clumping equilibrium in carbonate-substituted apatite was created to provide an independent temperature calibration. This model is based on a B-type carbonate substitution into fluorapatite—where a CO_3^{2-} group replaces one PO_4^{3-} group in each unit cell. To maintain charge balance, one Na^+ ion is substituted for a Ca^{2+} in each unit cell as well. B-type substitution is thought to be the dominant mechanism for incorporating carbonate in biogenic apatites (1), although it is less clear whether Na^+ for Ca^{2+} is the main charge-balancing substitution. Fluorapatite is chosen because it has a simpler unit cell than hydroxylapatite (e.g., 2), facilitating density-functional theory calculations. One carbonate group per unit cell (out of six phosphate sites) corresponds to ~4.5% wt. CO_2 in the structure, similar to biogenic apatites (1, 3).

Much like conventional stable isotope fractionations, ^{13}C-^{18}O clumping equilibria are controlled mainly by vibrational energy differences between isotopically substituted species (isotopologues) in an isotope exchange reaction; i.e.,

$$(^{13}C^{16}O_3^{2-})Ap + (^{12}C^{18}O^{16}O_2^{2-})Ap \leftarrow$$
$$\rightarrow (^{12}C^{16}O_3^{2-})Ap + (^{13}C^{18}O^{16}O_2^{2-})Ap$$

Where $(^xC^yO^{16}O_2^{2-})Ap$ is the relevant isotopologous substitution in apatite. These equilibria can be successfully estimated if a suitable model of the vibrational (phonon) frequencies of each isotopologue can be generated (4, 5). In the case of apatite, where carbonate is a minor nonstoichiometric substituent, a structural model for the carbonate substitution is needed before vibrational frequencies can be calculated.

Modeling Method. The positions of substituted CO_3^{2-} and Na^+ groups in the model fluorapatite structure are determined by an initial empirical-potential optimization followed by electronic structure calculations using density-functional theory (DFT). Initial optimization was performed in the General Utility Lattice Program (GULP; 6), using a previously generated empirical-potential model (7). We attempted to survey all symmetrically distinct Na-compensated B-type substitution configurations. Initial guess carbonate $\leftarrow\rightarrow$ phosphate replacement structures were generated by substituting one carbon atom for phosphorus and deleting one oxygen atom at a time in the same PO_4^{3-} group. Each guess configuration was allowed to relax under constant-volume then constant-pressure constraints (10^5 Pa). Among the relaxed structures, the lowest potential energy was observed when Na^+ substituted into the Ca(2) site—which shares bonds with fluoride in pure fluorapatite and hydroxyl groups in hydroxyapatite—and the oxygen vacancy was located on a phosphatic O(2) or O(3) site nearby. Three of the thirty tested configurations shared indistinguishable calculated lattice energies (−446.6303 eV/unit cell), the lowest in the survey. These three structures were crystallographically equivalent after empirical-potential relaxation.

This minimum-energy substituted structure was then used as an initial guess structure in a DFT-based structural optimization using the Quantum Espresso package (8; www.quantum-espresso.org). Electronic structure calculations used the PBE gradient-corrected functional (9) and the plane-wave pseudopotentials C.pbe-rrkjus.UPF, O.pbe-rrkjus.UPF, F.pbe-n-van.UPF, Na.pbe-sp-van_ak.UPF, P.pbe-van_ak.UPF, and Ca.pbe-nsp-van.UPF, available from the www.quantum-espresso.org distribution. The plane-wave energy cutoff was set at 40 Rydberg, sufficient to obtain convergence of structural parameters within ~0.1%—test calculations at a cutoff energy of 50 Rydberg showed insignificant changes in the structure—as was also found for calcite and pure fluorapatite. One electronic wave vector is sampled, (0, 0, 1/2). Atomic positions and unit cell dimensions were allowed to relax until forces acting on each atom were less than 10^{-4} Rydberg/bohr (4×10^{-12} N) and stresses on the unit cell were less than 0.5 kbar. Fig. S5 and Table S5 show the resulting structure, compared to stoichiometric apatite. The carbonate group is coincident and coplanar with a mirror plane in the parent fluorapatite structure, consistent with the structural arrangement inferred from neutron powder diffraction measurements (10).

Phonon frequencies at zero phonon wave vector were then calculated for the resulting DFT-optimized structural model, assuming average atomic masses for each atom. The matrix of force constants generated in this calculation was then used to determine frequencies for each isotopologue in the exchange reaction, following the procedure of Schauble et al. 2006 (4). All three possible ^{18}O-substitution sites in the carbonate molecule were substituted in turn. Phonon frequencies are all positive real numbers, indicating that the optimized structure represents a local energy minimum at that unit cell size. Subsequent calculations at the (0, 0, 1/2) phonon wave vector suggest that this structure is dynamically unstable with respect to a supercell (doubled along the z-axis), consistent with positional disorder observed in actual apatites (10). Since isotopic ordering and fractionation properties are dominantly controlled by short-range valence bonding interactions (4) it is expected that the long-range ordering forces responsible for this instability are not very important in determining the clumping equilibrium. Indeed, the equilibrium constant calculated using all positive frequencies at the (0, 0, 1/2) phonon wave vector is within 3×10^{-7} (0.0003‰) of the (0, 0, 0) wave-vector estimate at 250 + °K.

Phonon frequencies calculated with the PBE functional tend to be lower than measured frequencies (4, 11). In order to correct for this, we calculated optimized crystal structures (Table S6) and zero wave-vector frequencies for calcite and pure fluorapatite, and compared them to infrared and Raman spectroscopic measurements. For calcite, the estimated frequency scale factor is 1.032 ± 0.004, very close to what was used in an earlier calculation of clumping equilibria. The best-fit scale factor for fluorapatite is somewhat larger, 1.055 ± 0.002. It seems most likely that this reflects slightly different systematic errors in force constants associated with internal vibrations of CO_3^{2-} vs. PO_4^{3-}, because the associated vibrational modes dominate the high-frequency part of each mineral's spectrum. Since ^{13}C-^{18}O clumping is dominantly controlled by internal vibrations of the carbonate molecule, the calcite scale factor is used. Substituting the average of the apatite and calcite scale factors would raise the estimated clumping K_{eq} by approximately 1×10^{-5} (0.01‰) at 25 °C.

Calculated phonon frequencies for all model structures are shown in Table S7.

K_{eq}(38) Calculated ^{13}C-^{18}O clumping equilibria (K_{eq}) are shown in Fig. 2. A polynomial fit is also given to facilitate interpolation between the reported temperature points.

Carbonate fluorapatite:

$$K_{eq}(38) = 1 - 8.5580 \times 10^{-3}/T + 2.3632/T^2 + 2.1480 \times 10^4/T^3 - 3.1506 \times 10^6/T^4$$

Calcite:

$$K_{eq}(38) = 1 - 6.6699 \times 10^{-3}/T - 1.1483/T^2 + 2.2466 \times 10^4/T^3 - 3.2146 \times 10^6/T^4$$

Where T is the absolute temperature. These polynomials reproduce calculated equilibrium constants within 3×10^{-6} at temperatures above 250 °K.

The positionally averaged K_{eq} of B-type carbonate-substituted fluorapatite is remarkably similar to the analogous calcite model, as well as to a previously described calcite model created with different software and pseudopotentials (4). As noted in that study, empirical calibrations suggest somewhat greater temperature sensitivity than first-principles models. All three models yield temperature estimates within 1–2 °C for a given Δ_{47} CO_2. The clumping vs. temperature relationship in carbonate-substituted apatite thus seems likely to be indistinguishable from calcite. As a theoretical matter this conclusion is tentative—it will be necessary to model alternate defect structures in both fluorapatite and hydroxyl apatite to examine possible heterogeneity—but it does support the empirically observed match between calcite and apatite calibrations.

1. Elliott JC (2002) Calcium Phosphate Biominerals. *Reviews in Mineralogy and Geochemistry. Phosphates: Geochemical, Geobiological, and Materials Importance.* Eds. Kohn MJ, Rakovan J, & Hughes JM (Mineralogical Society of America and Geochemical Society, Washington, DC), Vol 48, pp 427–453.
2. Elliott JC, Mackie PE, & Young RA (1973) Monoclinic hydroxyapatite. *Science* 180:1055–1057.
3. Vennemann TW, Hegner E, Cliff G, & Benz GW (2001) Isotopic composition of recent shark teeth as a proxy for environmental conditions. *Geochim Cosmochim Acta* 65 (10):1583–1599.
4. Schauble EA, Ghosh P, & Eiler JM (2006) Preferential formation of ^{13}C-^{18}O bonds in carbonate minerals, estimated using first-principles lattice dynamics. *Geochim Cosmochim Acta* 70(10):2510–2529.
5. Wang Z, Schauble E, & Eiler JM (2004) Equilibrium thermodynamics of multiply-substituted isotopologues of molecular gases. *Geochim Cosmochim Acta* 68 (23):4779–4797.
6. Gale JD & Rohl AL (2003) The general utility lattice program. *Mol Simulat* 29:291–341.
7. Rabone JAL & De Leeuw NH (2006) Interatomic potential models for natural apatite crystals: Incorporating strontium and lanthanides. *J Comput Chem* 27:253–266.
8. Giannozzi P et al. (2009) QUANTUM ESPRESSO: A modular and open-source software project for quantum simulations of materials. *J Phys-Condens Mat* 21(39):395502.
9. Perdew JP, Burke K, & Ernzerhof M (1996) Generalized gradient approximation made simple. *Phys Rev Lett* 77:3865–3868.
10. Leventouri TH, Chakoumakos BC, Papanearchou N, & Perdikatsis V (2001) Comparison of crystal structure parameters of natural and synthetic apatites from neutron powder diffraction. *J Mater Res* 16:2600–2606.
11. Wu Z & Cohen RE (2006) More accurate generalized gradient approximation for solids. *Phys Rev B* 73:235116.
12. von Koenigswald W (1988) Paleoclimatic implication of the last glacial mammals from the northern upper Rhine plain (Translated from German). *About the paleoclimatology of the last interglacial in the northern part of the upper Rhine plain* (Translated from German). Ed. Koenigswald Wv (Akademie der Wissenschaften und der Literatur., Mainz), pp 205–314.
13. von Koenigswald W (2002) *Living Ice Age* (Translated from German). (Theiss Verlag, Stuttgart) p 190.
14. Tütken T, Vennemann TW, & Pfretzschner H-U (2008) Early diagenesis of bone and tooth apatite in fluvial and marine settings: Constraints from combined oxygen isotope, nitrogen, and REE analysis. *Palaeogeogr Palaeoclimatol Palaeoecol* 266(3-4):254–268.
15. Kohn MJ & Cerling TE (2002) Stable isotope compositions of biological apatite. *Reviews in Mineralogy and Geochemistry. Phosphates: Geochemical, Geobiological, and Materials Importance.* Eds. Kohn MJ, Rakovan J, & Hughes JM (Mineralogical Society of America and Geochemical Society., Washington, DC.), Vol 48, pp 455–488.
16. Koch PL, Tuross N, & Fogel ML (1997) The effects of sample treatment and diagenesis on the isotopic integrity of carbonate in biogenic hydroxyapatite. *J Archaeol Sci* 24 (5):417–429.
17. Ghosh P et al. (2006) ^{13}C-^{18}O bonds in carbonate minerals: a new kind of paleothermometer. *Geochim Cosmochim Acta* 70(6):1439–1456.
18. Graf DL (1961) Crystallographic tables for the rhombohedral carbonates. *Am Mineral* 46:1283–1316.
19. Comodi P, Liu Y, Zanazzi PF, & Montagnoli M (2001) Structural and vibrational behaviour of fluorapatite with pressure. Part I: In situ single-crystal X-ray diffraction investigation. *Phys Chem Miner* 28(4):219–224.
20. Cowley ER & Pant AK (1973) Lattice dynamics of calcite. *Phys Rev B* 8(10):4795–4800.
21. Hellwege KH, Lesch W, Plihal M, & Schaack G (1977) Two phonon absorption spectra and dispersion of phonon branches in crystals of calcite structure (Translated from German). *Zeitschrift fur Physik* 232:61–86.
22. Porto SPS (1966) Depolarization of Raman scattering in calcite. *Phys Rev* 147:608–611.
23. Pilati T, Demartin F, & Gramaccioli CM (1998) Lattice-dynamical estimation of atomic displacement parameters in carbonates: Calcite and aragonite $CaCO_3$, dolomite $CaMg(CO_3)_2$ and magnesite $MgCO_3$. *Acta Crystallogr B*54:515–523.
24. Leroy G, Penel G, Leroy N, & Brès E (2002) Human tooth enamel: a Raman polarized approach. *Appl Spectrosc* 56:1030–1034.

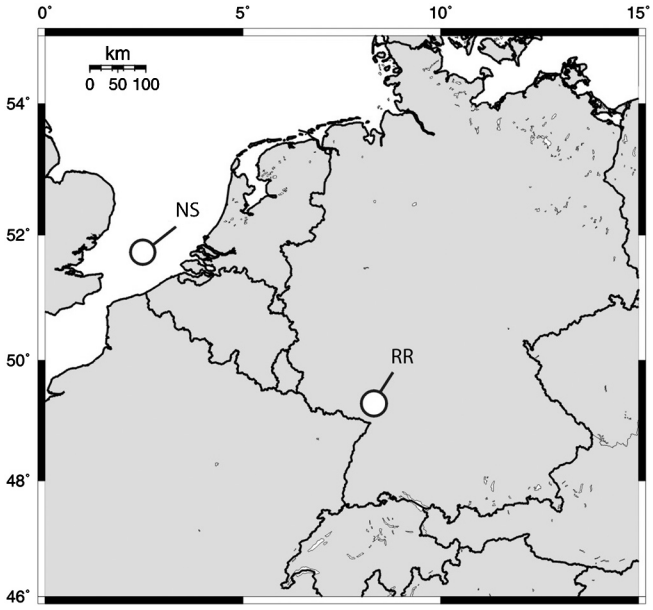

Fig. S1. Fossil mammoth tooth localities. The specimens of mammoth teeth analyzed in this study were obtained from two localities; the Rhine River gravels (RR) and the North Sea (NS). Geologic details of these Pleistocene deposits are described elsewhere (12, 13). The North Sea is a shallow continental shelf sea, and during the Last Glacial Maximum sea level was at least 120 meters lower, exposing the whole region and accounting for the presence of terrestrial fauna at this site. This locality is thought to have been flooded during the Holocene, at ~8 ka before present (14).

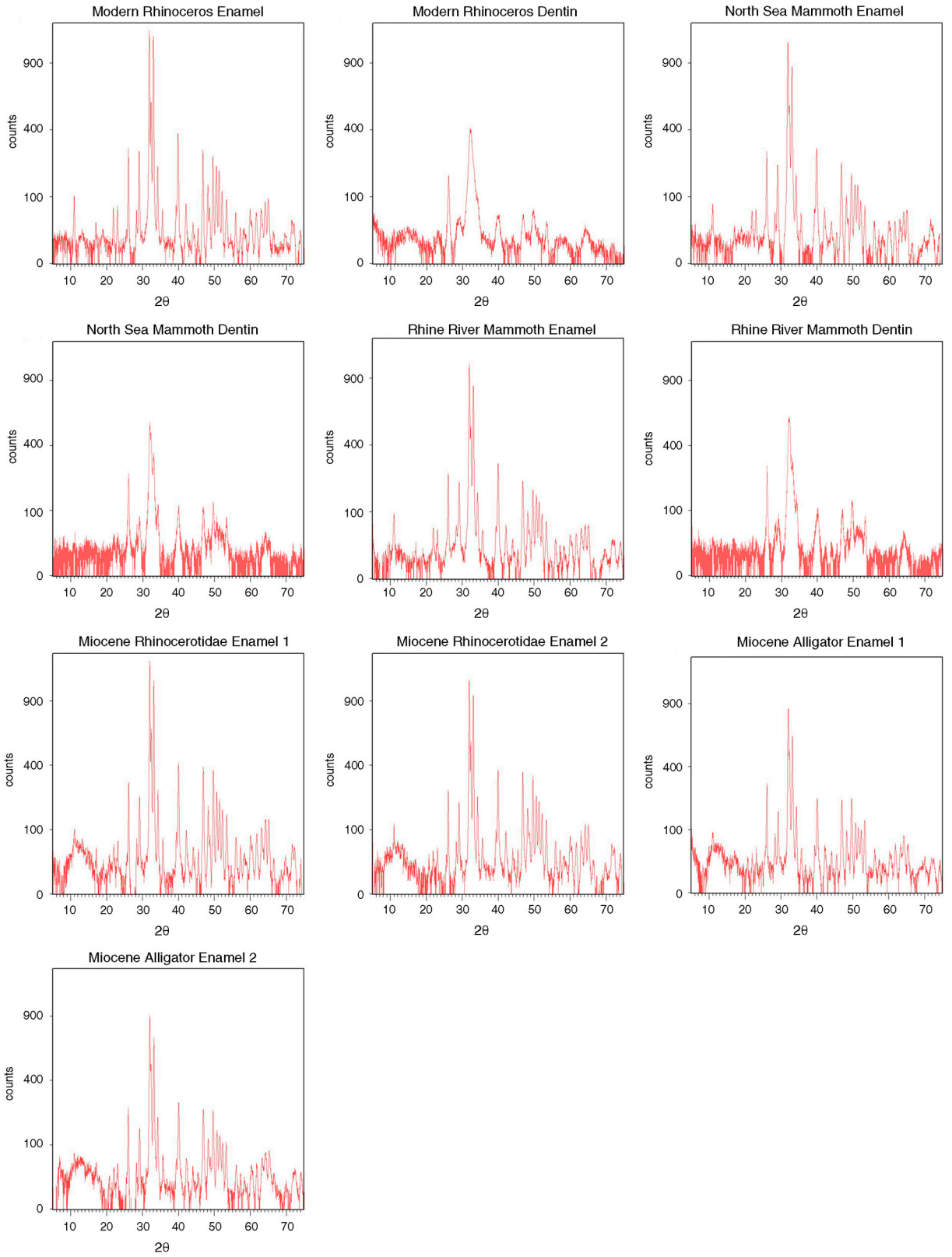

Fig. S2. X-ray diffraction spectra of modern and fossil bioapatite. No significant difference in peak shape is observed in the fossil material compared to modern. We also obtained data on modern rhinoceros enamel and dentin before sample pretreatment steps, giving spectra that were indistinguishable from the results presented here and are omitted in the interests of brevity.

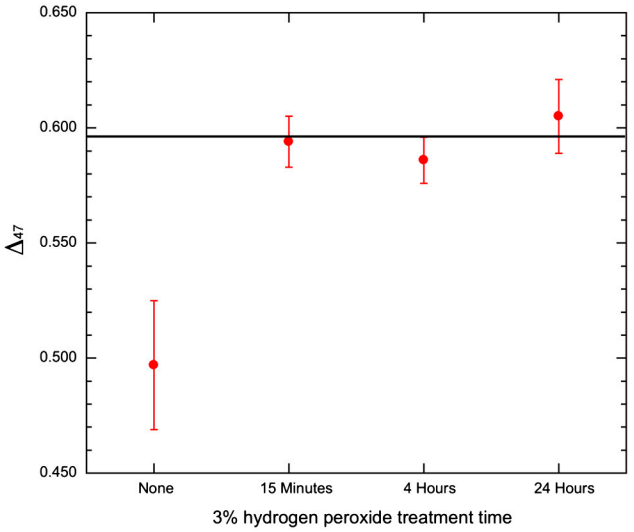

Fig. S3. The influence of 3% hydrogen peroxide (H_2O_2) treatment on Δ_{47} measurements from modern rhinoceros tooth enamel bioapatite. In the isotopic analysis of bioapatite an oxidative step is normally included to remove organic matter, which can be present at relatively high levels in these biogenic minerals (15, 16). In this case we chose 3% hydrogen peroxide as a reagent. The horizontal line is drawn at 0.596, the Δ_{47} value predicted for calcite grown at 37 °C (the average body temperature of most mammals) by the temperature relationship defined by Ghosh et al. 2006 (17). Error bars represent the internal precision of the measurement to two standard errors. All treatment times give Δ_{47} values within error of the expected value for inorganic calcite. Untreated enamel was the exception to this, giving a significantly different Δ_{47} value. From this we concluded that a short hydrogen peroxide wash was necessary to remove organic material and achieve accurate Δ_{47} values. While 15 minutes appeared sufficient for this sample we chose a four-hour treatment for every other analysis in this study, as it is possible that other samples could have higher levels of organic contamination than the sample analyzed here. Raw data are given in Table S3.

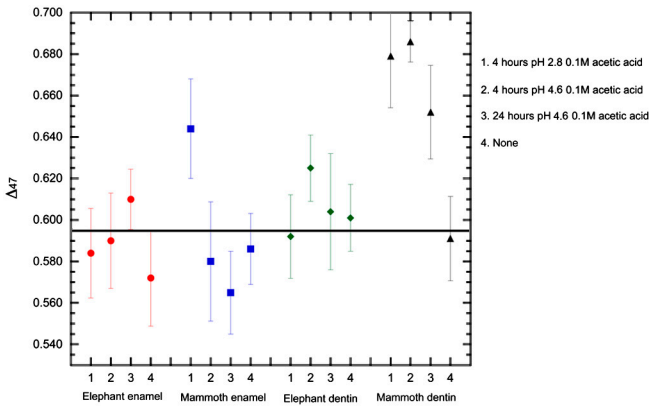

Fig. S4. The effects of acid washing on Δ_{47} measurements from modern and fossil tooth enamel and dentin. Acid washes are widely used in the stable isotope analysis of bioapatite in order to selectively dissolve "labile" and secondary carbonates, whilst leaving the original carbonate and phosphate components intact (15, 16). However, excessive acid washing can risk altering the structural carbonate in a sample (15, 16). The horizontal line represents the Δ_{47} value expected for inorganic calcite grown at 37 °C. All samples were prewashed for 4 hours in 3% H_2O_2, raw data is given in Table S3. In the case of the samples there was no clear difference between 4 hour and 24 hour washes in pH4.6 0.1 M acetic acid. pH2.8 0.1 M acetic acid seemed to have an adverse effect on fossil tooth Δ_{47} in that both mammoth enamel and dentin measurements were not close to the 37 °C inorganic calcite line. As a result we chose to pool data from 4 and 24 hour pH4.6 0.1 M acetic acid treatments in the mammoth body temperature calculation in Table 2, but did not use pH 2.8 acid wash in other analyes. Strikingly even the mildest acetic acid wash significantly affected the Δ_{47} measurements from fossil dentin, but did not affect the enamel. Dentin is thought to be more susceptible to alteration than enamel, and so may well have more secondary carbonate present (15, 16). The observed effect of acid treatment on fossil dentin could arise from a kinetically driven isotope effect caused by partial dissolution of secondary carbonates, where lighter isotopologues of CO_3 dissolve more rapidly than heavier isotopologues leaving the mineral phase enriched in ^{13}C-^{18}O bonds.

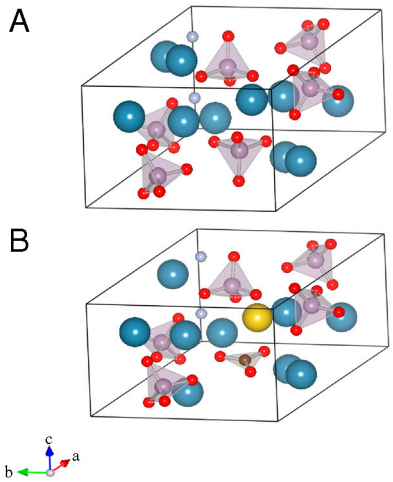

Fig. S5. Optimized structures of *A*) Carbonate-substituted fluorapatite, compared with *B*) Unsubstituted fluorapatite. During optimization of the substituted structure, one calcium atom migrated across the cell boundary, so it appears near the top of the cell in *A*) rather than near the bottom.

Other Supporting Information Files

Table S1 (DOC)
Table S2 (DOC)
Table S3 (DOC)
Table S4 (DOC)
Table S5 (DOC)
Table S6 (DOC)
Table S7 (DOC)